

DualToken: Towards Unifying Visual Understanding and Generation with Dual Visual Vocabularies

Wei Song^{1,2,3,5} Yuran Wang^{1,6} Zijia Song² Yadong Li¹ Haoze Sun¹ Weipeng Chen¹
 Zenan Zhou^{1*} Jianhua Xu^{1*} Jiaqi Wang^{4,5*} Kaicheng Yu^{2*}

¹ Baichuan Inc. ² Westlake University ³ Zhejiang University

⁴ Shanghai AI Laboratory ⁵ Shanghai Innovation Institute ⁶ Wuhan University

Abstract

The differing representation spaces required for visual understanding and generation pose a challenge in unifying them within the autoregressive paradigm of large language models. A vision tokenizer trained for reconstruction excels at capturing low-level perceptual details, making it well-suited for visual generation but lacking high-level semantic representations for understanding tasks. Conversely, a vision encoder trained via contrastive learning aligns well with language but struggles to decode back into the pixel space for generation tasks. To bridge this gap, we propose **DualToken**, a method that unifies representations for both understanding and generation within a single tokenizer. However, directly integrating reconstruction and semantic objectives in a single tokenizer creates conflicts, leading to degraded performance in both reconstruction quality and semantic performance. Instead of forcing a single codebook to handle both semantic and perceptual information, **DualToken** disentangles them by introducing separate codebooks for high and low-level features, effectively transforming their inherent conflict into a synergistic relationship. As a result, **DualToken** achieves state-of-the-art performance in both reconstruction and semantic tasks while demonstrating remarkable effectiveness in downstream MLLM understanding and generation tasks. Notably, we also show that **DualToken**, as a unified tokenizer, surpasses the naive combination of two distinct types vision encoders, providing superior performance within a unified MLLM. The code and models will be available at <https://github.com/songwei/DualToken>.

1. Introduction

Unifying visual understanding and generation within the autoregressive paradigm of large language models (LLMs) has become a current research hotspot, giving rise to representative works like CM3leon [54], Chameleon [40], Emu3

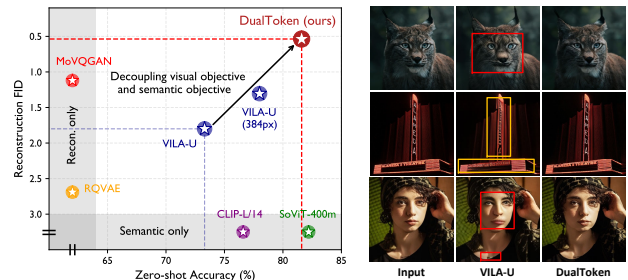


Figure 1. **Comparison with state-of-the-art vision encoders.** (Left) We compare zero-shot classification accuracy and reconstruction FID on ImageNet-1K(val) across baseline methods and DualToken. DualToken achieves results comparable to or surpassing both semantic-only and reconstruction-only methods in both tasks. (Right) Reconstruction results of VILA-U and DualToken, our DualToken significantly outperforms VILA-U, which suffers from severe distortion and blurriness.

[45] and VILA-U [47]. To achieve multimodal autoregressive generation, these unified models require a visual tokenizer to discretize visual inputs and a corresponding detokenizer to map tokens back to the pixel space.

Early methods [40, 45, 54] directly used the encoder and decoder of VQVAE as the tokenizer and detokenizer. However, although these methods successfully demonstrated the feasibility of unifying visual understanding and generation within the autoregressive paradigm, their understanding capabilities are typically lacking compared to traditional multimodal large language models (MLLMs) that specialize in understanding tasks [12, 20, 29, 31, 32, 38, 55, 58]. We argue that this decline in visual understanding performance stems from the insufficient visual representations—traditional VQVAE pre-training focuses on reconstruction tasks, making its embedding space rich in low-level visual information, but lack higher-level semantic knowledge. In contrast, MLLMs designed for understanding tasks [2, 23, 24, 26–28, 30, 44, 48] typically utilize CLIP-family encoders [1, 35, 56] to extract visual features. Since these

Table 1. **Comparison to state-of-the-art visual encoders or tokenizers.** For semantic metrics, we measured ImageNet zero-shot classification accuracy, as well as Text-to-Image/Image-to-Text retrieval (R@1) on Flickr8K. For reconstruction, we measured reconstruction FID (rFID), PSNR, and SSIM on ImageNet-1K (Val). Our method not only outperforms VILA-U and achieves performance comparable to the state-of-the-art SigLIP ViT-SO400M model in semantic metrics, but also mitigates the structural distortion and blurriness issues faced by VILA-U during reconstruction. Our method also surpasses dedicated models such as MoVQGAN in reconstruction metrics, reaching state-of-the-art performance.

VISION ENCODER (TOKENIZER)	Semantic			Reconstruction		
	Zero-Shot [†]	T2I(R@1) [†]	I2T(R@1) [†]	rFID [↓]	PSNR [†]	SSIM [†]
VQGAN [11]	×	×	×	4.98	-	-
MoVQGAN [59]	×	×	×	1.12	22.42	0.673
RQ-VAE [19]	×	×	×	2.69	-	-
ViT-VQGAN [52]	×	×	×	1.55	-	-
Open-MAGViT2 [33, 53]	×	×	×	1.17	21.90	-
SBER-MoVQGAN [37]	×	×	×	0.68	27.04	0.741
FQGAN-Dual (↓16) [3]	×	×	×	0.94	22.02	-
FQGAN-Triple (↓16) [3]	×	×	×	0.76	22.73	-
clip-ViT-L-14-336 [35]	76.6	21.15	21.50	×	×	×
siglip-so400m-14-384 [56]	82.1	21.70	21.60	×	×	×
VILA-U [47]	73.3	10.02	11.15	1.80	3.43	0.489
VILA-U [47] (SO400M)	78.0	-	-	1.25	-	-
DualToken (↓16) (ours)	81.6	21.05	21.55	0.54	23.56	0.742

encoders are pretrained with language alignment, their representations inherently capture high-level semantic information, making them more suitable for downstream visual understanding tasks in MLLMs.

To fully leverage the text-aligned semantic representations of CLIP, a natural approach is to quantize the features of a CLIP encoder and train a corresponding decoder for image reconstruction [47]. Specifically, this requires the visual tokenizer to learn reconstruction for downstream generation tasks while preserving its semantic capabilities as much as possible [47]. However, as shown in Fig.1 and Table1, directly combining reconstruction and semantic objectives often leads to severe distortions and blurriness in reconstruction tasks, along with a noticeable decline in semantic metrics such as zero-shot classification and image-text retrieval, compared to its original pretrained model [56]. This degradation, as discussed in [47], reflects the inherently conflict between the two training objectives, ultimately limiting both the quality of downstream image generation tasks and the performance of multimodal understanding tasks.

To decouple the two conflicting objectives effectively, we propose using two sets of visual vocabularies—High-Level (Semantic) and Low-Level (Perceptual)—to tokenize semantic and texture features separately. Specifically, similar to the hierarchical structure of the human vision system [16], the shallow-layer features of a ViT focus on perceptual-level texture information, while high-level semantic representations emerge in the deeper layers [6]. We argue that this inherent property of ViT should be fully

leveraged: using shallow-layer features for reconstruction and deep-layer features for semantic learning, thereby obtaining the texture and semantic codebook simultaneously.

Surprisingly, this hierarchical decoupling not only resolves the conflict between the two objectives but also enables the semantic learning objective to enhance low-level reconstruction. Moreover, training the shallow-layer reconstruction task does not compromise the model’s original semantic capabilities, even without additional contrastive learning stages [35, 47]. Building upon this, we further demonstrate how a multimodal large language model (MLLM) can effectively utilize the dual visual vocabularies to achieve unified vision understanding and generation.

2. Related Work

Unified Multimodal Large Language Models A common strategy for integrating visual understanding and generation within a single MLLM is to externally connect an LLM with a Diffusion Model [9, 13, 14, 39]. However, pure autoregressive (AR) architectures offer a more elegant, fully end-to-end solution by unifying both tasks within the same autoregressive framework. Representative models like Chameleon [40, 54] and Emu3 [45], have demonstrated the feasibility of jointly modeling vision and language through a unified next-token prediction objective. Specifically, visual inputs are first discretized into visual tokens with a vision tokenizer. These visual tokens are then interleaved with text tokens to construct a multimodal sequence. However, pure AR architectures like Chameleon introduce generative capabilities at the cost of significantly weaker visual understanding compared to models specifically designed for understanding tasks. An empirical explanation for this [47, 50] is that models like Chameleon typically utilize VQVAE [11, 43] encoders as their vision tokenizers. Since VQVAE is trained with a reconstruction objective, its encoder primarily extracts low-level visual features optimized for generation rather than the high-level semantic representations required for vision-language understanding. Therefore, improving the vision-language understanding performance of AR-based models necessitates a vision tokenizer that effectively captures both low-level representations for generation and high-level semantic representations for understanding.

Recent research has actively explored solutions in this direction. VILA-U [47] and MUSE-VL [50] strive to build a unified tokenizer by jointly training on both reconstruction and semantic objectives. However, due to the inherent disparity between semantic and texture features, they struggle to strike an optimal balance between the two objectives, resulting in subpar performance in both tasks. As discussed in FQGAN [3], decomposing the codebook in a divide-and-conquer manner may offer a more fundamental solution to this conflict. TokenFlow [34] employs separate codebooks

with a shared-mapping mechanism. However, key differences set our approach apart. First, TokenFlow relies on distinct vision towers to extract semantic and low-level features, rather than leveraging a unified architecture. Second, the shared IDs obtained through the shared-mapping mechanism may not be the optimal matches for either semantics or texture, potentially introducing additional losses in both domains. TokenFlow has yet to demonstrate its effectiveness in a unified MLLM setting that supports both generation and understanding; instead, it trains separate models dedicated to each task.

3. Method

This section formally introduces the design of our unified tokenizer and explains how its dual visual codebooks are utilized within the next-token prediction paradigm of LLMs for unified multimodal understanding and generation.

3.1. Motivation

As discussed in [34], CLIP-based encoders cluster images based on semantic similarity, whereas VQVAE-based encoders group images by low-level attributes such as color and texture. This suggests that encoders trained for reconstruction primarily extract low-level perceptual information, while CLIP-family encoders, pretrained with language alignment, inherently capture high-level semantic information. We argue that this difference in representation space plays a crucial role in downstream MLLM performance.

To validate this viewpoint, we started by a preliminary experiment following the LLaVA-1.5 pipeline [27]. As shown in Table 2, compared to the original SigLIP model, encoders trained with reconstruction objective exhibit a significant drop in downstream MLLM vision-language understanding performance, validating that high-level semantic features are more critical for visual reasoning in MLLMs than low-level perceptual features. However, to achieve both visual understanding and generation within a single MLLM, it is essential to decode the visual tokens back into pixel space as accurately as possible. However, since the SigLIP encoder focuses on high-level semantic information rather than texture details, simply discretizing its features and training a decoder without tuning the encoder results in poor image reconstruction quality. Therefore, proposing a unified tokenizer is crucial to enable high-quality visual understanding and generation within a single MLLM.

3.2. Unified Vision Tokenizer with Dual Codebooks

To build a unified tokenizer, we started with the simplest approach, where we directly combine the reconstruction loss and semantic loss to optimize the entire vision tower and use a single visual vocabulary to tokenize its feature, similar to VILA-U [47]. Specifically, as illustrated in Fig.2 (left), we initialize the vision encoder with pretrained weights from

Table 2. **Downstream visual understanding performance with different vision encoders within the LLaVA-1.5 framework.** *ViT-SO400M (pretrained)* refers to the original pretrained siglip-so400m-14-384 model [1], while *ViT-SO400M (recon.)* refers to the encoder that follows the same architecture but is trained solely for reconstruction from scratch, controlling for factors like model size and architecture.

Vision Encoder	MMB	MME	SEED	VQAv2	Zero-Shot	rFID
ViT-SO400M (pretrained)	61.8	1492.9	56.8	78.5	82.1	✗
ViT-SO400M (recon.)	36.2	822.4	30.6	47.5	✗	0.96
SBER-MoVQGAN-270M	35.8	792.0	34.1	45.2	✗	0.68

siglip-so400m-patch14-384 [1] to ensure strong text-image alignment. Then the semantic loss is computed between the deeper-layer features of the model and its initial state to constrain the model from losing its semantic capability.

However, as shown in Table.3(a), this straightforward approach leads to a clear conflict between the two objectives. On one hand, although the semantic loss is applied to preserve the model’s original semantic representation capabilities, achieving this objective proves difficult, as semantic performance metrics show a significant decline compared to the original model, reflecting the disruption caused by the reconstruction training objective on semantic capabilities. On the other hand, the model also struggles to achieve satisfactory reconstruction quality, often resulting in distortions and blurriness in the reconstructed images (Fig.2).

To address this, we decouple the learning of the reconstruction and semantic objectives through a hierarchical approach, as shown in Fig.2 (right). Specifically, reconstruction loss is applied to supervise the shallow layers (1-6) of the vision tower, while semantic loss is applied to the deeper layers (layer 26 and the pooling head). Features from the shallow and deep layers are then discretized separately via residual vector quantization [19], resulting in low-level and high-level visual vocabularies.

We utilize an Exponential Moving Average (EMA) strategy [36, 42] to update the codebook. To enhance codebook utilization, we implement a restart strategy where a cluster within the codebook is randomly replaced with an input from the current batch if it remains unused for a certain number of steps. To ensure the encoder outputs align closely with the codebook entries, we utilize a Vector Quantization (VQ) commitment loss, which is defined as:

$$\mathcal{L}_c = \|z - \text{quantize}(z)\|_2^2 \quad (1)$$

Consequently, the total loss is formulated as a weighted sum of reconstruction loss, semantic loss, and VQ commitment loss

$$\mathcal{L}_{total} = \lambda_1 \cdot \mathcal{L}_{recon} + \lambda_2 \cdot \mathcal{L}_{sem} + \lambda_3 \cdot (\mathcal{L}_{c1} + \mathcal{L}_{c1}) \quad (2)$$

where the reconstruction loss is the combination of pixel-wise L_2 loss [10], LPIPS loss [57] and adversarial loss [18]

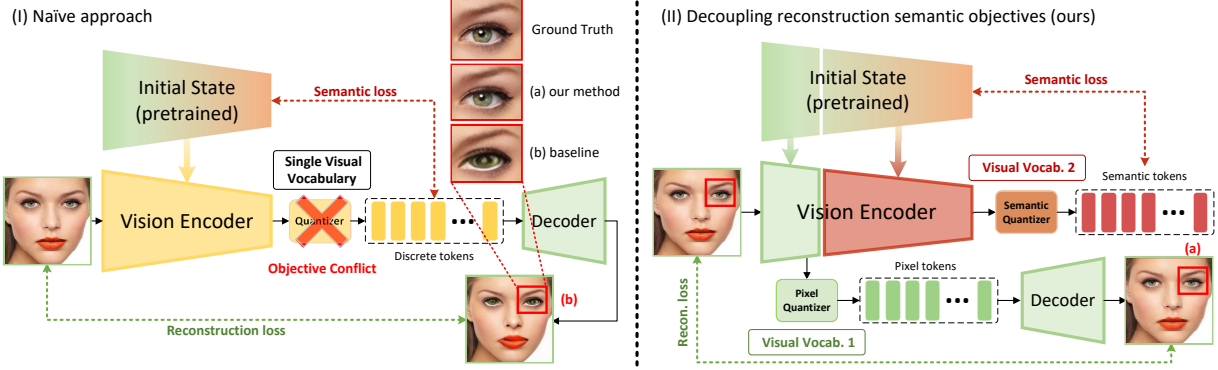


Figure 2. **Overview of our unified vision tokenizer.** Given input images the features extracted by the vision encoder are discretized using residual quantization. Then the discrete vision features are meanwhile put into the vision decoder to reconstruct images and used to perform the text-image alignment. During this process, the reconstruction loss and contrastive loss are computed to update the vision tower, endowing it to produce discrete visual features with text alignment.

Table 3. **DualToken transforms the conflict between reconstruction and semantic objectives into a synergistic relationship.** Directly combining the two objectives leads to a drastic decline in reconstruction performance (a vs. b). However, incorporating reconstruction and semantic losses hierarchically results in better reconstruction performance compared to using reconstruction alone as the target (d vs. c). We highlight our method in the last row.

# Exp.	Loss Type (layer)	Zero-Shot Acc. [↑]	Reconstruction		
			rFID [↓]	PSNR [↑]	SSIM [↑]
Initial State:					
		82.1			
(a)	Recon. (26) + Sem. (26)	75.2	4.36	11.85	0.579
(b)	Recon. (26)	✗	0.71	21.88	0.640
(c)	Recon. (6)	✗	0.73	22.12	0.680
(d)	Recon. (6) + Sem. (26)	81.6	0.54	23.56	0.742

for reconstructing an input image:

$$\mathcal{L}_{recon} = \|\hat{x} - x\|_2^2 + \lambda_p \mathcal{L}_{LPIPS}(\hat{x}, x) + \lambda_g \mathcal{L}_G(\hat{x}) \quad (3)$$

while the semantic loss is simply computed as the L_2 distance between the model’s 26th-layer feature representation F and its corresponding initial state F_0

$$\mathcal{L}_{sem} = \|F - F_0\|_2^2 \quad (4)$$

Interestingly, as shown in Table.3 (d), even without adding an additional contrastive learning phase to enhance semantic capabilities and relying solely on a simple L_2 loss to constrain the semantic representation, incorporating a reconstruction learning objective in our hierarchical learning strategy causes minimal damage to the model’s semantic ability. More intriguingly, as shown in Table.3 (b), (c), and (d), compared to training solely for reconstruction, learning the semantic objective in the deeper layers actually enhances the reconstruction task in the shallow layers, successfully transforming the conflict between semantic and reconstruction objectives into a positive relationship.

3.3. Unifying Understanding and Generation

In this section, we demonstrate how to integrate the dual visual codebooks of DualToken within a unified MLLM. As illustrated in Fig. 3 (c), to model both textual and visual content under the autoregressive paradigm of LLMs, the pixel and semantic visual tokens are first concatenated along their embedding dimension to form unified visual tokens. These unified visual tokens are then concatenated with text tokens to construct a multimodal token sequence. Then the model is trained in an autoregressive manner to predict the next token for both visual and textual tokens. For simplicity, we define the language vocabulary of our MLLM as a finite set $\mathcal{X} = \{x_1, x_2, \dots, x_{n_1}\}$, while the low-level and high-level visual vocabulary as $\mathcal{Y} = \{y_1, y_2, \dots, y_{n_2}\}$ and $\mathcal{Z} = \{z_1, z_2, \dots, z_{n_3}\}$, where n_1 , n_2 , and n_3 represent the vocabulary sizes for language tokens, low-level visual tokens, and high-level visual tokens, respectively.

For visual tokens, since residual quantization introduces a depth-stacked structure of codes at each visual position p , we implement our visual heads based on the depth transformer from RQ-VAE [19]. Unlike the original depth transformer, which employs a single head to predict logits across all depths, we introduce separate classification heads to compute the logits for residuals at each corresponding depth [21]. Specifically, the high-level semantic tokens and low-level pixel tokens are processed by independent visual heads—the pixel head and the semantic head—as shown in Fig.3. Both heads share the same structure, comprising three layers of depth transformers (each with a depth of 8) and eight classification heads.

Given the LLM hidden state h_p for visual tokens at position p , our depth transformer autoregressively predicts D residual tokens $(r_{p1}, r_{p2}, \dots, r_{pD})$. For $d > 1$, the input to the depth transformer at depth d , denoted as I_{pd} , is defined

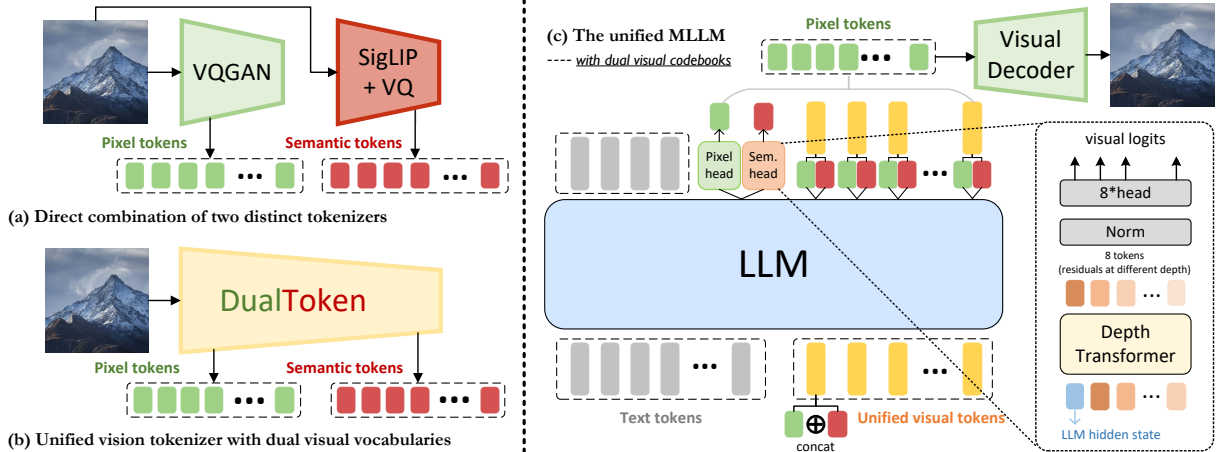


Figure 3. **An overview of our framework utilizing dual visual codebooks for unified visual understanding and generation.** (a) Directly using VQGAN and SigLIP to separately acquire high-level (semantic) and low-level (pixel) visual codebooks. (b) Our approach: decoupling high-level and low-level visual codebooks within a unified vision tokenizer. The image is converted into low-level visual tokens (green) and text-aligned semantic tokens (red). (c) To model both textual and visual content within the autoregressive paradigm of LLMs, the pixel and semantic visual tokens are first concatenated along their embedding dimension to form unified visual tokens (yellow). These unified visual tokens are then concatenated with text tokens to construct a multimodal token sequence. The model is trained to predict the next token for both visual and textual tokens. Specifically, the high-level and low-level visual tokens are processed by independent visual heads (Pixel head and Semantic head), each comprising a depth transformer (3 layers with a depth of 8) and 8 classification heads to predict the residuals of the corresponding visual token at different depths. During inference, the generated low-level tokens are decoded by our visual decoder to reconstruct the visual content.

as the sum of the token embeddings of up to depth $d - 1$

$$I_{pd} = \sum_{d'=1}^{d-1} \mathbf{e}(r_{pd'}), \quad (5)$$

where $r \in \mathcal{Y}$ for the pixel head and $r \in \mathcal{Z}$ for the semantic head. The initial input at depth 1 is given by $I_{p1} = h_p$. This formulation ensures that the depth transformer incrementally refines the predicted feature representation by leveraging previous estimations up to depth $d - 1$. Consequently, the overall negative log-likelihood loss for the entire multimodal sequence of length N is defined as

$$\mathcal{L}_{\text{NTP}} = - \sum_{i=1}^N \mathcal{P}_i \quad (6)$$

where,

$$\mathcal{P}_i = \log P(x_i | x_{<i}) \quad (7)$$

if a text token appears at position i , and

$$\mathcal{P}_i = \sum_{d=1}^D [\log P(y_{id} | y_{i,<d}) + \log P(z_{id} | z_{i,<d})] \quad (8)$$

if visual tokens appears at position i . During multimodal pretraining, the weights of the depth transformers are randomly initialized and trained jointly with the LLM. During inference, only the low-level tokens are utilized by our visual decoder to reconstruct the visual content.

4. Experiments

In this section, we present a comprehensive set of experiments to assess our method across a range of visual understanding and generation tasks. We begin by detailing our experimental setup. Next, we analyze the performance of our unified vision tokenizer. Finally, we benchmark our approach against leading MLLMs, showcasing its strengths in both visual understanding and generation. However, please note that this research is still ongoing, and the final results, complete metrics, and additional technical details may be updated before the final release.

4.1. Experimental Setup

We utilize Qwen-2.5-3B [51] as the base language model and adopt the pretrained weights from the SigLIP-SO400M-patch14-384 [1] for our visual tokenizer. All images are resized to 384×384 and transformed into $27 \times 27 \times 8$ semantic or pixel tokens, with a residual depth of $D = 8$. Our vision tokenizer is trained on CC12M [4] and evaluated for zero-shot classification and reconstruction performance on ImageNet [8]. We evaluate our model against widely used vision-language understanding benchmarks, including VQAv2 [15], POPE [22], MME [12], SEED-IMG [20], MMBench [29], and MM-Vet [55]. For visual generation, we apply classifier-free guidance [17] with a CFG value of 3 to enhance the quality of generated outputs.

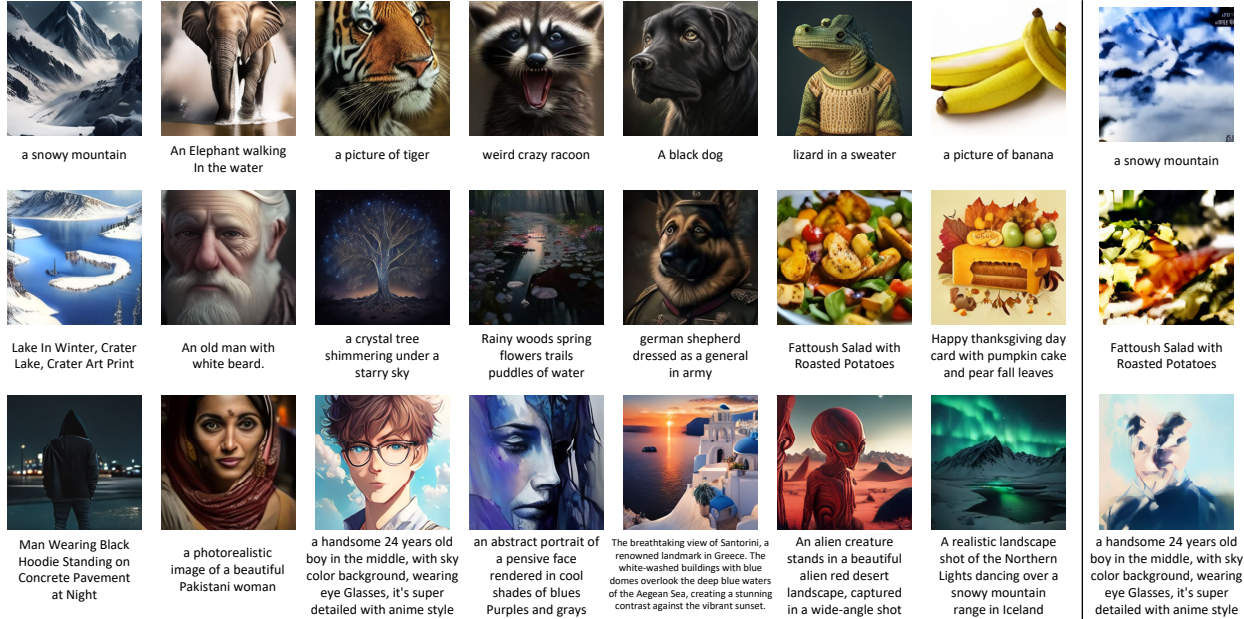


Figure 4. **Visual generation results with DualToken.** (Left) Our DualToken can generate high-quality images given text input. (Right) Following the pipeline introduced in Fig. 3 (a), we experimented with using the codebook of SBER-MoVQGAN as the low-level vocabulary and the codebook of a VQ-processed SigLIP as the high-level vocabulary, while keeping the same method and training data for downstream MLLM training. However, this straightforward approach results in significantly poorer image generation performance.

4.2. Vision Tokenizer

For evaluating the semantic capabilities of our unified vision tokenizer, we report the Top-1 accuracy for zero-shot image classification on ImageNet-1K (validation set), along with text-to-image and image-to-text retrieval performance (R@1) on Flickr8K. As shown in Table 1, our DualToken significantly outperforms VILA-U in both classification and retrieval tasks, while also surpassing the dedicated CLIP-L-14-336 model in zero-shot image classification. Notably, thanks to our hierarchical decoupling approach, DualToken achieves semantic performance on par with the state-of-the-art SigLIP ViT-SO400M-14-384 model, without requiring any additional stages specifically designed to enhance semantic capabilities. We believe that incorporating an additional contrastive learning stage—where the shallow layers responsible for reconstruction are frozen while only the deeper layers are optimized for semantic objective—could further enhance the model’s semantic performance.

To evaluate reconstruction capability, we measured reconstruction FID (rFID), PSNR, and SSIM on the ImageNet-1K validation set. Our DualToken achieves the highest structural similarity and the lowest rFID among various state-of-the-art dedicated methods, including OpenMAGViT2 [33] and SBER-MoVQGAN [37]. This demonstrates that our method effectively mitigates the structural distortion and blurriness issues encountered by VILA-U during reconstruction.

Table 4. **Controlled experiment on various vision-language understanding benchmarks.** We evaluate different vision encoders/tokenizers, including siglip-so400m-14-384, VILA-U, and DualToken within the LLaVA-1.5 framework. MMB denotes MMBench-dev.

Vision Encoder	MMB	VQAv2	POPE	MME	SEED	MMVet
siglip-so400-patch14-384	61.8	78.5	85.9	1492.9	56.8	36.0
VILA-U	56.3(-5.5)	74.1(-4.4)	83.5(-2.4)	1301.4(-191.5)	52.2(-4.6)	25.9(-10.1)
DualToken (sem.+pcept.)	64.5(+2.7)	78.3(-0.2)	86.1(+0.2)	1589.6(+96.7)	58.9(+2.1)	37.8(+1.8)
DualToken (sem.)	61.2(-0.6)	77.8(-0.7)	84.8(-1.1)	1495.8(+2.9)	57.2(+0.4)	35.4(-0.6)

4.3. Downstream Performance

Visual Understanding Model. Before formally presenting the performance of our unified model, we first conducted a controlled experiment to validate the effectiveness of our vision tokenizer in downstream MLLM visual understanding tasks. To ensure a fair comparison by controlling factors such as training data, model size, and architecture, we evaluate the downstream visual understanding performance of DualToken within the LLaVA-1.5 [27] framework. Specifically, we replace the vision encoder of LLaVA-1.5 with DualToken, while strictly adhering to its training data and using LLaMA-2-7B [41] as the foundational LLM. As shown in Table 4, our DualToken, as a discrete unified vision tokenizer, outperforms VILA-U and even surpasses the original continuous SigLIP model when used as the vision encoder. More interestingly, we conducted separate experiments using only the semantic tokens

Table 5. **Evaluation on multimodal understanding benchmarks.** Our DualToken (3B) demonstrates strong performance compared to other unified models and achieves results comparable to dedicated understanding models like LLaVA-NeXT and ShareGPT4V. Note that the latest version is still in training, and the metrics may be updated before the final release.

Type	Method	# LLM Params	POPE	MMBench	SEED	MMMU	MMVet	MathVista	MME
<i>Und.</i>	InstructBLIP [7]	7B	-	36.0	58.8	30.6	26.2	24.4	1137.1
	LLaVA-Phi [60]	2.7B	85.0	59.8	-	-	28.9	-	1335.1
	LLaVA-1.5 [27]	7B	85.9	64.3	58.6	35.4	31.1	27.4	1510.7
	LLaVA-NeXT [28]	7B	86.5	67.4	70.2	35.8	43.9	34.6	1519.0
	LLaVA-NeXT [28]	34B	87.7	79.3	75.9	51.1	57.4	46.5	1631.0
	ShareGPT4V [5]	7B	-	68.8	69.7	37.2	37.6	26.5	1567.4
	VILA [25]	7B	85.5	68.9	61.1	-	34.9	-	1533.0
<i>Uni.</i>	DreamLLM [9]	7B	-	58.2	-	-	36.6	-	-
	SEEDLLaMA [13]	7B	-	45.8	51.5	-	-	-	-
	Chameleon [40]	7B	-	31.1	-	22.4	8.3	-	-
	Emu3 [45]	8B	85.2	58.5	68.2	31.6	-	-	-
	Show-o [49]	1.5B	73.8	-	-	25.1	-	-	948.4
	Janus [46]	1.5B	87.0	69.4	63.7	30.5	34.3	-	1338.0
	MUSE-VL [50]	7B	-	72.1	70.0	42.3	-	52.5	1480.9
	VILA-U [47]	7B	85.8	-	59.0	-	33.5	-	1401.8
	DualToken (ours)	3B	86.0	70.9	70.2	38.6	32.5	46.5	1489.2

(sem.), extracted from the 26th layer, as well as a combination of semantic tokens and pixel tokens (sem.+pcpt), concatenated along the embedding dimension as visual input. Compared to using semantic tokens alone, jointly leveraging semantic and pixel tokens generally leads to better performance across various visual reasoning benchmarks, such as MMBench [29] and MME [12]. This highlights that low-level texture features are not only essential for generation tasks but also contribute positively to enhancing the model’s visual understanding capabilities.

Unified Model for Generation and Understanding. We further implemented our unified MLLM framework for both visual understanding and generation based on the method introduced in Sec.3.3 and Fig.3, where separate visual heads predict semantic and pixel tokens. As shown in Table 5, our DualToken (3B) demonstrates strong performance compared to other unified models and achieves results comparable to dedicated understanding models like LLaVA-NeXT and ShareGPT4V. Meanwhile, as illustrated in Fig. 4, our unified model can generate visually compelling content from text input. The generated images exhibit remarkable alignment with the text, even for long and complex prompts. Thanks to the high reconstruction quality of DualToken, the generated images are rich in detail and structurally realistic, accurately capturing fine textures such as animal fur, water waves, and other intricate patterns.

To further answer a basic question: why do we need to obtain dual visual vocabularies within a unified tokenizer rather than simply combining existing specialized encoders? We experimented with using the codebook of SBER-MoVQGAN as the low-level vocabulary and the codebook of a VQ-processed SigLIP as the high-level vo-

cabulary, while keeping the same method and training data for downstream MLLM training. As shown in Fig. 4 (right), this straightforward approach results in significantly poorer image generation performance, further demonstrating the importance of obtaining dual visual vocabularies within a unified visual tokenizer. It is also worth noting that this simple combination approach differs from Janus [46], whose semantic encoder operates continuously without tokenization and only serves as the encoder for understanding tasks, without being involved in the visual generation process.

5. Conclusion

In summary, our contributions are threefold: (i) Decoupling Reconstruction and Semantic Objectives: We successfully disentangle reconstruction and semantic learning objectives through a hierarchical approach, transforming their inherent conflict into a beneficial relationship. (ii) Dual Visual Codebooks for Enhanced Understanding and Generation: We demonstrate that employing dual visual codebooks outperforms single-codebook approaches in both understanding and generation tasks. (iii) A Unified Model for Vision Understanding and Generation: We propose a viable paradigm for unifying vision understanding and generation using dual visual codebooks. However, this work represents only a baseline implementation of this paradigm, leaving ample room for further exploration. Notably, prior unified models for understanding and generation have not demonstrated clear mutual reinforcement between these tasks. A key direction is to investigate the potential of fully leveraging dual visual codebooks to achieve genuine synergy between visual understanding and generation.

Important Note Please note that this research is still in progress. The final results, complete metrics, and additional technical details are scheduled to be updated in due course.

References

- [1] Ibrahim M Alabdulmohsin, Xiaohua Zhai, Alexander Kolesnikov, and Lucas Beyer. Getting vit in shape: Scaling laws for compute-optimal model design. *Advances in Neural Information Processing Systems*, 36:16406–16425, 2023. 1, 3, 5
- [2] Jinze Bai, Shuai Bai, Shusheng Yang, Shijie Wang, Sinan Tan, Peng Wang, Junyang Lin, Chang Zhou, and Jingren Zhou. Qwen-vl: A versatile vision-language model for understanding, localization, text reading, and beyond, 2023. 1
- [3] Zechen Bai, Jianxiong Gao, Ziteng Gao, Pichao Wang, Zheng Zhang, Tong He, and Mike Zheng Shou. Factorized visual tokenization and generation. *arXiv preprint arXiv:2411.16681*, 2024. 2
- [4] Soravit Changpinyo, Piyush Sharma, Nan Ding, and Radu Soricut. Conceptual 12M: Pushing web-scale image-text pre-training to recognize long-tail visual concepts. In *CVPR*, 2021. 5
- [5] Lin Chen, Jinsong Li, Xiaoyi Dong, Pan Zhang, Conghui He, Jiaqi Wang, Feng Zhao, and Dahua Lin. Sharegpt4v: Improving large multi-modal models with better captions. In *European Conference on Computer Vision*, pages 370–387. Springer, 2024. 7
- [6] Yongjie Chen, Hongmin Liu, Haoran Yin, and Bin Fan. Building vision transformers with hierarchy aware feature aggregation. In *Proceedings of the IEEE/CVF International Conference on Computer Vision*, pages 5908–5918, 2023. 2
- [7] Wenliang Dai, Junnan Li, Dongxu Li, Anthony Meng Huat Tiong, Junqi Zhao, Weisheng Wang, Boyang Li, Pascale Fung, and Steven Hoi. Instructblip: Towards general-purpose vision-language models with instruction tuning, 2023. 7
- [8] Jia Deng, Wei Dong, Richard Socher, Li-Jia Li, Kai Li, and Li Fei-Fei. Imagenet: A large-scale hierarchical image database. In *2009 IEEE conference on computer vision and pattern recognition*, pages 248–255. Ieee, 2009. 5
- [9] Runpei Dong, Chunrui Han, Yuang Peng, Zekun Qi, Zheng Ge, Jinrong Yang, Liang Zhao, Jianjian Sun, Hongyu Zhou, Haoran Wei, Xiangwen Kong, Xiangyu Zhang, Kaisheng Ma, and Li Yi. DreamLLM: Synergistic multimodal comprehension and creation. In *The Twelfth International Conference on Learning Representations*, 2024. 2, 7
- [10] Alexey Dosovitskiy and Thomas Brox. Generating images with perceptual similarity metrics based on deep networks. *Advances in neural information processing systems*, 29, 2016. 3
- [11] Patrick Esser, Robin Rombach, and Bjorn Ommer. Taming transformers for high-resolution image synthesis. In *Proceedings of the IEEE/CVF conference on computer vision and pattern recognition*, pages 12873–12883, 2021. 2
- [12] Chaoyou Fu, Peixian Chen, Yunhang Shen, Yulei Qin, Mengdan Zhang, Xu Lin, Jinrui Yang, Xiawu Zheng, Ke Li, Xing Sun, Yunsheng Wu, and Rongrong Ji. Mme: A comprehensive evaluation benchmark for multimodal large language models, 2024. 1, 5, 7
- [13] Yuying Ge, Sijie Zhao, Ziyun Zeng, Yixiao Ge, Chen Li, Xintao Wang, and Ying Shan. Making llama see and draw with seed tokenizer. *arXiv preprint arXiv:2310.01218*, 2023. 2, 7
- [14] Yuying Ge, Sijie Zhao, Jinguo Zhu, Yixiao Ge, Kun Yi, Lin Song, Chen Li, Xiaohan Ding, and Ying Shan. Seed-x: Multimodal models with unified multi-granularity comprehension and generation. *arXiv preprint arXiv:2404.14396*, 2024. 2
- [15] Yash Goyal, Tejas Khot, Douglas Summers-Stay, Dhruv Batra, and Devi Parikh. Making the V in VQA matter: Elevating the role of image understanding in Visual Question Answering. In *Conference on Computer Vision and Pattern Recognition (CVPR)*, 2017. 5
- [16] Iris IA Groen, Edward H Silson, and Chris I Baker. Contributions of low-and high-level properties to neural processing of visual scenes in the human brain. *Philosophical Transactions of the Royal Society B: Biological Sciences*, 372(1714): 20160102, 2017. 2
- [17] Jonathan Ho and Tim Salimans. Classifier-free diffusion guidance. *arXiv preprint arXiv:2207.12598*, 2022. 5
- [18] Phillip Isola, Jun-Yan Zhu, Tinghui Zhou, and Alexei A Efros. Image-to-image translation with conditional adversarial networks. In *Proceedings of the IEEE conference on computer vision and pattern recognition*, pages 1125–1134, 2017. 3
- [19] Doyup Lee, Chiheon Kim, Saehoon Kim, Minsu Cho, and Wook-Shin Han. Autoregressive image generation using residual quantization. In *Proceedings of the IEEE/CVF Conference on Computer Vision and Pattern Recognition*, pages 11523–11532, 2022. 2, 3, 4
- [20] Bohao Li, Rui Wang, Guangzhi Wang, Yuying Ge, Yixiao Ge, and Ying Shan. Seed-bench: Benchmarking multimodal llms with generative comprehension. *arXiv preprint arXiv:2307.16125*, 2023. 1, 5
- [21] Tianpeng Li, Jun Liu, Tao Zhang, Yuanbo Fang, Da Pan, Mingrui Wang, Zheng Liang, Zehuan Li, Mingan Lin, Guosheng Dong, et al. Baichuan-audio: A unified framework for end-to-end speech interaction. *arXiv preprint arXiv:2502.17239*, 2025. 4
- [22] Yifan Li, Yifan Du, Kun Zhou, Jinpeng Wang, Wayne Xin Zhao, and Ji-Rong Wen. Evaluating object hallucination in large vision-language models. *arXiv preprint arXiv:2305.10355*, 2023. 5
- [23] Yadong Li, Haoze Sun, Mingan Lin, Tianpeng Li, Guosheng Dong, Tao Zhang, Bowen Ding, Wei Song, Zhenglin Cheng, Yuqi Huo, Song Chen, Xu Li, Da Pan, Shusen Zhang, Xin Wu, Zheng Liang, Jun Liu, Tao Zhang, Keer Lu, Yaqi Zhao, Yanjun Shen, Fan Yang, Kaicheng Yu, Tao Lin, Jianhua Xu, Zenan Zhou, and Weipeng Chen. Baichuan-omni technical report. *arXiv preprint arXiv:2410.08565*, 2024. 1
- [24] Yadong Li, Jun Liu, Tao Zhang, Song Chen, Tianpeng Li, Zehuan Li, Lijun Liu, Lingfeng Ming, Guosheng Dong, Da Pan, et al. Baichuan-omni-1.5 technical report. *arXiv preprint arXiv:2501.15368*, 2025. 1

- [25] Ji Lin, Hongxu Yin, Wei Ping, Pavlo Molchanov, Mohammad Shoeybi, and Song Han. Vila: On pre-training for visual language models. In *Proceedings of the IEEE/CVF conference on computer vision and pattern recognition*, pages 26689–26699, 2024. 7
- [26] Haotian Liu, Chunyuan Li, Qingyang Wu, and Yong Jae Lee. Visual instruction tuning. *Advances in neural information processing systems*, 36:34892–34916, 2023. 1
- [27] Haotian Liu, Chunyuan Li, Yuheng Li, and Yong Jae Lee. Improved baselines with visual instruction tuning. In *Proceedings of the IEEE/CVF Conference on Computer Vision and Pattern Recognition*, pages 26296–26306, 2024. 3, 6, 7
- [28] Haotian Liu, Chunyuan Li, Yuheng Li, Bo Li, Yuanhan Zhang, Sheng Shen, and Yong Jae Lee. Llava-next: Improved reasoning, ocr, and world knowledge, 2024. 1, 7
- [29] Yuan Liu, Haodong Duan, Yuanhan Zhang, Bo Li, Songyang Zhang, Wangbo Zhao, Yike Yuan, Jiaqi Wang, Conghui He, Ziwei Liu, et al. Mmbench: Is your multi-modal model an all-around player? *arXiv preprint arXiv:2307.06281*, 2023. 1, 5, 7
- [30] Haoyu Lu, Wen Liu, Bo Zhang, Bingxuan Wang, Kai Dong, Bo Liu, Jingxiang Sun, Tongzheng Ren, Zhuoshu Li, Hao Yang, Yaofeng Sun, Chengqi Deng, Hanwei Xu, Zhenda Xie, and Chong Ruan. Deepseek-vl: Towards real-world vision-language understanding, 2024. 1
- [31] Pan Lu, Swaroop Mishra, Tanglin Xia, Liang Qiu, Kai-Wei Chang, Song-Chun Zhu, Oyvind Tafjord, Peter Clark, and Ashwin Kalyan. Learn to explain: Multimodal reasoning via thought chains for science question answering. *Advances in Neural Information Processing Systems*, 35:2507–2521, 2022. 1
- [32] Pan Lu, Hritik Bansal, Tony Xia, Jiacheng Liu, Chunyuan Li, Hannaneh Hajishirzi, Hao Cheng, Kai-Wei Chang, Michel Galley, and Jianfeng Gao. Mathvista: Evaluating mathematical reasoning of foundation models in visual contexts. *arXiv preprint arXiv:2310.02255*, 2023. 1
- [33] Zhuoyan Luo, Fengyuan Shi, Yixiao Ge, Yujiu Yang, Limin Wang, and Ying Shan. Open-magvit2: An open-source project toward democratizing auto-regressive visual generation. *arXiv preprint arXiv:2409.04410*, 2024. 2, 6
- [34] Liao Qu, Huichao Zhang, Yiheng Liu, Xu Wang, Yi Jiang, Yiming Gao, Hu Ye, Daniel K Du, Zehuan Yuan, and Xinglong Wu. Tokenflow: Unified image tokenizer for multimodal understanding and generation. *arXiv preprint arXiv:2412.03069*, 2024. 2, 3
- [35] Alec Radford, Jong Wook Kim, Chris Hallacy, Aditya Ramesh, Gabriel Goh, Sandhini Agarwal, Girish Sastry, Amanda Askell, Pamela Mishkin, Jack Clark, et al. Learning transferable visual models from natural language supervision. In *International conference on machine learning*, pages 8748–8763, 2021. 1, 2
- [36] Ali Razavi, Aaron Van den Oord, and Oriol Vinyals. Generating diverse high-fidelity images with vq-vae-2. *Advances in neural information processing systems*, 32, 2019. 3
- [37] SberBank. Sber-movqgan, 2023. 2, 6
- [38] Wei Song, Yadong Li, Jianhua Xu, Guowei Wu, Lingfeng Ming, Kexin Yi, Weihua Luo, Houyi Li, Yi Du, Fangda Guo, et al. M3gia: A cognition inspired multilingual and multimodal general intelligence ability benchmark. *arXiv preprint arXiv:2406.05343*, 2024. 1
- [39] Quan Sun, Yufeng Cui, Xiaosong Zhang, Fan Zhang, Qiyang Yu, Yueze Wang, Yongming Rao, Jingjing Liu, Tiejun Huang, and Xinlong Wang. Generative multimodal models are in-context learners. In *Proceedings of the IEEE/CVF Conference on Computer Vision and Pattern Recognition*, pages 14398–14409, 2024. 2
- [40] Chameleon Team. Chameleon: Mixed-modal early-fusion foundation models. *arXiv preprint arXiv:2405.09818*, 2024. 1, 2, 7
- [41] Hugo Touvron, Louis Martin, Kevin Stone, Peter Albert, Amjad Almahairi, Yasmine Babaei, Nikolay Bashlykov, Soumya Batra, Prajjwal Bhargava, Shruti Bhosale, et al. Llama 2: Open foundation and fine-tuned chat models. *arXiv preprint arXiv:2307.09288*, 2023. 6
- [42] Aaron Van Den Oord, Oriol Vinyals, et al. Neural discrete representation learning. *Advances in neural information processing systems*, 30, 2017. 3
- [43] Aaron Van Den Oord, Oriol Vinyals, et al. Neural discrete representation learning. *Advances in neural information processing systems*, 30, 2017. 2
- [44] Peng Wang, Shuai Bai, Sinan Tan, Shijie Wang, Zhihao Fan, Jinze Bai, Keqin Chen, Xuejing Liu, Jialin Wang, Wenbin Ge, Yang Fan, Kai Dang, Mengfei Du, Xuancheng Ren, Rui Men, Dayiheng Liu, Chang Zhou, Jingren Zhou, and Junyang Lin. Qwen2-vl: Enhancing vision-language model’s perception of the world at any resolution. *arXiv preprint arXiv:2409.12191*, 2024. 1
- [45] Xinlong Wang, Xiaosong Zhang, Zhengxiong Luo, Quan Sun, Yufeng Cui, Jinsheng Wang, Fan Zhang, Yueze Wang, Zhen Li, Qiyang Yu, et al. Emu3: Next-token prediction is all you need. *arXiv preprint arXiv:2409.18869*, 2024. 1, 2, 7
- [46] Chengyue Wu, Xiaokang Chen, Zhiyu Wu, Yiyang Ma, Xingchao Liu, Zizheng Pan, Wen Liu, Zhenda Xie, Xingkai Yu, Chong Ruan, et al. Janus: Decoupling visual encoding for unified multimodal understanding and generation. *arXiv preprint arXiv:2410.13848*, 2024. 7
- [47] Yecheng Wu, Zhuoyang Zhang, Junyu Chen, Haotian Tang, Dacheng Li, Yunhao Fang, Ligeng Zhu, Enze Xie, Hongxu Yin, Li Yi, et al. Vila-u: a unified foundation model integrating visual understanding and generation. *arXiv preprint arXiv:2409.04429*, 2024. 1, 2, 3, 7
- [48] Zhiyu Wu, Xiaokang Chen, Zizheng Pan, Xingchao Liu, Wen Liu, Damai Dai, Huazuo Gao, Yiyang Ma, Chengyue Wu, Bingxuan Wang, Zhenda Xie, Yu Wu, Kai Hu, Jiawei Wang, Yaofeng Sun, Yukun Li, Yishi Piao, Kang Guan, Aixin Liu, Xin Xie, Yuxiang You, Kai Dong, Xingkai Yu, Haowei Zhang, Liang Zhao, Yisong Wang, and Chong Ruan. Deepseek-vl2: Mixture-of-experts vision-language models for advanced multimodal understanding, 2024. 1
- [49] Jinheng Xie, Weijia Mao, Zechen Bai, David Junhao Zhang, Weihao Wang, Kevin Qinghong Lin, Yuchao Gu, Zhijie Chen, Zhenheng Yang, and Mike Zheng Shou. Show-o: One single transformer to unify multimodal understanding and generation. *arXiv preprint arXiv:2408.12528*, 2024. 7

- [50] Rongchang Xie, Chen Du, Ping Song, and Chang Liu. Muse-vl: Modeling unified vlm through semantic discrete encoding. *arXiv preprint arXiv:2411.17762*, 2024. 2, 7
- [51] An Yang, Baosong Yang, Beichen Zhang, Binyuan Hui, Bo Zheng, Bowen Yu, Chengyuan Li, Dayiheng Liu, Fei Huang, Haoran Wei, et al. Qwen2.5 technical report. *arXiv preprint arXiv:2412.15115*, 2024. 5
- [52] Jiahui Yu, Xin Li, Jing Yu Koh, Han Zhang, Ruoming Pang, James Qin, Alexander Ku, Yuanzhong Xu, Jason Baldridge, and Yonghui Wu. Vector-quantized image modeling with improved vqgan. *arXiv preprint arXiv:2110.04627*, 2021. 2
- [53] Lijun Yu, José Lezama, Nitesh B Gundavarapu, Luca Versari, Kihyuk Sohn, David Minnen, Yong Cheng, Vighnesh Birodkar, Agrim Gupta, Xiuye Gu, et al. Language model beats diffusion—tokenizer is key to visual generation. *arXiv preprint arXiv:2310.05737*, 2023. 2
- [54] Lili Yu, Bowen Shi, Ramakanth Pasunuru, Benjamin Muller, Olga Golovneva, Tianlu Wang, Arun Babu, Binh Tang, Brian Karrer, Shelly Sheynin, et al. Scaling autoregressive multi-modal models: Pretraining and instruction tuning. *arXiv preprint arXiv:2309.02591*, 2023. 1, 2
- [55] Weihao Yu, Zhengyuan Yang, Linjie Li, Jianfeng Wang, Kevin Lin, Zicheng Liu, Xinchao Wang, and Lijuan Wang. Mm-vet: Evaluating large multimodal models for integrated capabilities. *arXiv preprint arXiv:2308.02490*, 2023. 1, 5
- [56] Xiaohua Zhai, Basil Mustafa, Alexander Kolesnikov, and Lucas Beyer. Sigmoid loss for language image pre-training. In *Proceedings of the IEEE/CVF international conference on computer vision*, pages 11975–11986, 2023. 1, 2
- [57] Richard Zhang, Phillip Isola, Alexei A Efros, Eli Shechtman, and Oliver Wang. The unreasonable effectiveness of deep features as a perceptual metric. In *Proceedings of the IEEE conference on computer vision and pattern recognition*, pages 586–595, 2018. 3
- [58] Wenxuan Zhang, Mahani Aljunied, Chang Gao, Yew Ken Chia, and Lidong Bing. M3exam: A multilingual, multi-modal, multilevel benchmark for examining large language models, 2024. 1
- [59] Chuanxia Zheng, Tung-Long Vuong, Jianfei Cai, and Dinh Phung. Movq: Modulating quantized vectors for high-fidelity image generation. *Advances in Neural Information Processing Systems*, 35:23412–23425, 2022. 2
- [60] Yichen Zhu, Minjie Zhu, Ning Liu, Zhiyuan Xu, and Yaxin Peng. Llava-phi: Efficient multi-modal assistant with small language model. In *Proceedings of the 1st International Workshop on Efficient Multimedia Computing under Limited*, pages 18–22, 2024. 7